

Continuous-time Data-Based Mechanistic (DBM) Models and Their Importance in a Changing Environment

Peter C. Young

Lancaster Environment Centre and the Data Science Institute,
Lancaster University, UK

Abstract

In most areas of forecasting and time series analysis, discrete-time black-box models, that are so well known in the forecasting community, provide an important tool in understanding and forecasting the behavior of dynamic systems. On the other hand, in most areas of science and engineering, continuous-time differential models have been the normal means of describing such dynamic systems since the time of Newton and Leibniz. In this scientific and engineering context, as well as in other areas such as macro-economics, models are not only meant for characterizing patterns in data for purposes such as forecasting. Normally, a clear physical interpretation is also required to provide scientific credibility and help make decisions that require a knowledge of the system's internal behavior, such as fault or behavioural diagnosis, monitoring the changes in physical characteristics, scenario analysis and making 'management' decisions. Continuous-time models have significant advantages in these kind of applications. The paper starts with a philosophical discussion about the differences between inductive and hypothetico-deductive methods in modeling and how 'hypothetico-inductive' data-based mechanistic (HI-DBM) modeling relates to these. Readers who may be relatively unacquainted with the continuous-time models are provided with a background to this subject by the inclusion of an appendix. This provides a short introduction to transfer function models (the algebraic operator representation of differential equations) for linear and nonlinear systems; as well as outlining how such models are statistically identified and recursively estimated from time series data using computational routines that are freely available in the CAPTAIN Toolbox for MatlabTM. However, the main part of the paper, following the philosophical discussion, shows how such continuous-time HI-DBM models and methods are applied in practice, with two important examples where they have been used recently: one on the study of climate change; and the other on the monitoring and forecasting of the COVID-19 epidemic.

Keywords: Hybrid continuous-time Box-Jenkins model, optimal recursive instrumental variable (RIV/RIVC) estimation, climate change, COVID-19 epidemic, monitoring, forecasting, fixed interval smoothing, dynamic harmonic regression (DHR), dynamic linear regression (DLR), state-dependent parameter (SDP) estimation

1. Introduction

Over many years, I have found it very strange that continuous-time, differential equation models are almost absent from the forecasting and time series analysis literature, particularly since such models are so important in science and engineering. Moreover, continuous-time modeling can be superior to discrete-time modeling. Unlike discrete-time models, where the parameter values are a function of the data sampling interval, continuous-time model parameters are normally independent of the sampling rate; they usually provide a unique description of the dynamic system;

they are physically meaningful; they often have associated units that enhance their meaning in such physical terms; and continuous-time models can work well with rapidly sampled and irregularly sampled data, where discrete-time models normally fail or have identifiability problems. In addition to these model advantages, optimal statistical tools for the identification and estimation of continuous-time models are freely available and are quite easy to apply to sampled time series data.

This paper concentrates on the continuous-time *Data-Based Mechanistic* (DBM) modeling of stochastic, dynamic systems from sampled time series data. This approach to modeling is illustrated well by its applica-

tion to two important problems that dominate humanity at the present time and are the main subject of this paper: climate change and the COVID-19 pandemic. First, section 3 discusses the modeling of the global climate change based on annual data over the period 1856 to 2015, concentrating on the identification of a DBM model that has a physically meaningful interpretation. The model is identified using continuous-time *Refined Instrumental Variable* (RIVC) estimation and it provides a tool for the estimation of important climate parameters, as well as for applications such as future scenario analysis and emissions management. The advantages of continuous-time modeling are particularly clear in this application where discrete-time models are unable to identify a model that can compete with the continuous-time model in either descriptive or statistical terms.

Section 4 is rather different. It provides a briefer description of recent research on the simple monitoring and forecasting of the COVID-19 epidemic. First, the ‘rate-of-change’ that is so important to the understanding of any dynamic system and occurs naturally in continuous-time models, is estimated indirectly, using time-variable parameter *Dynamic Harmonic Regression* (DHR). It then provides a continually updated, adaptive tool for monitoring and predicting the progress of the epidemic. After this, the same type of continuous-time transfer function model used in section 3 is employed for short-to-medium term forecasting of the epidemic in the UK.

At this point, those readers who may be relatively unacquainted with the continuous-time models can, if they so wish, peruse Appendix A. This provides an introduction to ‘transfer function’ models (the algebraic operator representation of differential equations) for linear systems; an outline of these models, together with the DHR model, within an unobserved component model framework; and a description of how such models are statistically identified and recursively estimated from time series data, using computational routines that are freely available in the CAPTAIN Toolbox for MatlabTM.

Before continuing to the examples discussed in section 3 and 4, the next section considers the philosophical background to DBM modeling, which stretches back at least to the 17th Century, when science was referred to as ‘natural philosophy’ and differential equations were just being developed as a tool to model dynamic systems from experimental and natural data.

2. The Philosophical Background

It is perhaps appropriate that, in the middle of the Covid-19 pandemic, I should be extolling the virtues of differential calculus and differential equation models of dynamic systems; concepts that were probably first suggested (in unpublished form) by Newton in 1666, during the great bubonic plague epidemic in the UK. Of course, there has been great controversy over who first invented this approach to modeling dynamic systems, Newton or Leibniz; and there were previous contributions that clearly influenced them (e.g. Newton refers back to Fermat’s *Methodus ad disquirendam maximam et minimam* and *De tangentibus linearum curvarum*). But there is no doubt that the nomenclature used for the exposition of differential equations that I will use in this paper, and which that has been used in science and engineering since the 17th Century, is that introduced by Leibniz. He began working on his variant of differential calculus in 1674, and published his first paper employing it *Nova Methodus pro Maximis et Minimis* in 1684¹.

However, my appreciation for Newton is not specifically for his work on the development of differential calculus. Rather it relates to the phrase ‘*Hypotheses non fingo*’, which appears in the concluding *Scholium Generale* of the revised second edition of the Principia (1713) and has been translated as ‘I frame no hypotheses’. While there has been some debate about this translation, there can be little doubt what views Newton held on the formulation of hypotheses when he says:

“As in Mathematicks, so in Natural Philosophy², the Investigation of difficult Things by the Method of Analysis, ought ever to precede the Method of Composition. This Analysis consists in making Experiments and Observations, and in drawing general Conclusions from them by Induction, and admitting of no Objections against the Conclusions, but such as are taken from Experiments, or other certain Truths. *For Hypotheses are not to be regarded in experimental Philosophy*³. ”

– Isaac Newton (1718). *Opticks, 2nd edition* (1718), Book 3, Query 31, 380.

¹In 1687, Newton explained his form of calculus in Book I of his *Philosophiae Naturalis Principia Mathematica* but did not publish his eventual ‘fluxional’ notation until later (partly in 1693 and fully in 1704).

²‘Natural Philosophy’ (from the Latin *philosophia naturalis*), is the term used to describe ‘science’ before the development of ‘modern’ science in the 19th Century and beyond

³my emphasis

The inductive approach to science and mathematical modeling preferred by Newton was not his invention: it has a long history in philosophy and had been discussed by Francis Bacon (1561-1626) and, almost contemporaneously with Newton, by Robert Boyle (1627-1691). Interestingly, the polymath William Whewell (1794-1866), who was actually born in Lancaster (the residence of my wife Wendy and I for the last 40 years), wrote two books on induction: *a History of the Inductive Sciences, from the Earliest to the Present Times* (1837) and *The Philosophy of the Inductive Sciences* (1840). And, believe it or not, he also introduced the terms ‘scientist’, and ‘physicist’.

The phrase ‘*Hypotheses non fingo*’ and its meaning was pointed out to me many years ago by the famous systems theorist Rudolf Kalman (see figure 1) and



Figure 1: The author and Rudolf Kalman, 1985 discussing Newton’s views on the dangers of hypotheses in scientific investigation.

it was discussed by him in a presentation, entitled ‘*I have a Friend*’ (the friend was Newton!), at a workshop that he organized for a few invitees at a palace on the shores of Lake Como. This influenced me to develop the *Data-Based Mechanistic* (DBM) approach to modeling⁴ that plays an important part in the present paper. Here, a data-based *inductive* procedure is followed and reliance on prior hypotheses is discouraged, with both the model structure and the parameters that characterize this structure inferred from available time series data obtained from the dynamic system under investigation, *often during its normal operation*. Hypotheses are not ignored but they are not allowed to prejudice the data-based modeling and are not considered seriously until *after* the model structure has been identified and its associated parameters estimated. I have

⁴‘Data-driven’ appears more popular these days but the meaning appears to be much the same.

referred to this as a *hypothetico-inductive* DBM modeling procedure (HI-DBM: see [41]), in order that it can be contrasted with the *hypothetico-deductive* approach espoused by the great philosopher of science Karl Popper [24], where the hypotheses drive the modeling and form the basis for model parameter estimation. However, the hypothetico-inductive approach does not reject all of Popper’s views. For instance, he suggests that one should not attempt to ‘prove’ a hypothesis but rather attempt its ‘falsification’; and then, if it is not falsified, consider it only to be ‘conditionally valid’. These suggestions are eminently sensible and are, therefore, absorbed into the hypothetico-inductive approach.

DBM modeling is, then, an inductive ‘method theory’. It has been developed over many years and its name emphasizes my contention that, while the model should be inferred inductively from the analysis of data in as objective a manner as possible, it should also have a clear, scientifically acceptable, mechanistic interpretation. In a very real sense, therefore, although DBM modeling exploits some of the methodology used in ‘black-box’ modeling, it is actually a reaction against the notion of pure black-box models. While such models provide an excellent vehicle for activities such as signal and image processing, or some aspects of statistical forecasting and automatic control, I believe they are not sufficient for scientific and engineering research that is attempting to investigate the nature of dynamic systems in the natural and man-made world. In other words, a model should not just explain the time series data well, it should also provide a mechanistic description of the system under investigation; a description that further enhances our confidence in its ability to approximate reality in a meaningful manner.

It is also important to note that DBM modeling was developed particularly for the analysis of measured data collected during the normal operation of the system, rather than from planned experiments on the system. The ability to perform experiments is very important in Popper’s view of scientific discovery. One only has to search for the word ‘experiment’ in his famous book to realize how important experimentation, and particularly planned experimentation, is in his view of the scientific method. As he says:

“Only when certain events recur in accordance with rules or regularities, as is the case with repeatable experiments, can our observations be tested ... We do not take even our own observations quite seriously, or accept them as scientific observations, until we have repeated and tested them. Only by such repe-

tions can we convince ourselves that we are not dealing with a mere isolated coincidence, but with events which, on account of their regularity and reproducibility, are in principle inter-subjectively testable”.

Unfortunately, it is rarely possible to conduct well-planned experiments on natural systems in order to remove the often inherent ambiguity in the observations and so clarify our understanding of the potentially complex mechanisms that underlie this observed behaviour. The climate scientist, for instance, can hypothesize about the causes and mechanisms of ‘global warming’ but it is clear from the controversy on this topic, that such hypotheses, although widely recognized in the scientific community, are not universally accepted in full. Even if we remove the ‘climate deniers’, who appear politically and economically motivated, there remains considerable debate about the rate of climate change and the nature and rapidity of changes, such as in the weather and sea levels, that one might expect. And this is clearly a situation where planned experimentation, that might help to resolve such ambiguities, is impossible.

My reaction against the over-use of Popper’s hypothetico-deductive approach to science is reinforced by the work of the other great 20th Century philosopher, Robert Kuhn [13]. He viewed science from a ‘paradigmatic’ standpoint in which most ‘ordinary science’ worked within and embroidered defined paradigms and hypotheses; while the more fundamental achievements of science were those that questioned, or even overturned, these current paradigms (as Einstein’s theories of relativity radically changed the Newtonian view of the World). In this regard, the hypothetico-deductive approach used by such ordinary scientists often tends to be too constrained by current paradigms: hypotheses are made within the current paradigm and do not often seek to question it. I hope, therefore, that Kuhn might have been sympathetic to my hypothetico-inductive views.

Finally, DBM modeling is not a pre-defined methodology applied in a similar way each time it is applied to a new dynamic system. Rather it is an ‘art and craft’ that requires careful and possibly novel data processing and modeling procedures when used to characterize the dynamic behaviour of real-World systems *in order to meet its specified objectives*. While the definition of such objectives is very important in all modeling, because there is rarely only one model for any given system, it is an essential pre-requisite for DBM modeling.

Of course, a crafts-person must have tools. Many of the tools required for DBM modeling are available in the *Computer-Aided Program for Time series Analysis and Identification of Noisy dynamic systems (CAPTAIN) Toolbox* for MatlabTM. These tools are numerical algorithms implemented by the CAPTAIN Toolbox routines; and they have been very influential in the development and refinement of DBM modeling over many years. The Toolbox can be downloaded free from <https://wp.lancs.ac.uk/captaintoolbox> and should then be placed appropriately in the Matlab path.

The craft of DBM modeling is, I feel, well illustrated by the DBM climate modeling that is discussed in the next section 3. Here a rather unusual approach is utilized for model identification and estimation; one that does not conform completely with the standard procedure for linear model identification and develops a customized method of statistically optimal parameter estimation.

3. Hypothetico-Inductive DBM Modeling of Global Climate Change

I first became interested in global climate modeling in 1996 (see e.g. [22, 29]) and continued, after the turn of the Millennium, with research on the modeling and control of global climate change, at first concentrating on modeling as an aid to emissions management (see [48, 11]). Although an agnostic at first, my initial analysis of the ‘leveling’ episode that occurred in the globally averaged temperature from around 2001, followed by renewed growth thereafter, encouraged me to investigate the nature of the relationship between *Total Radiative Forcing* (TRF): and the *Global surface Temperature Anomaly* (GTA) in more detail. Here, the TRF is the summation of all the radiative forcing inputs, including those caused by greenhouse gases, aerosols and volcanic activity, that affect global surface temperature.

This research convinced me that global warming was a real and potentially dangerous phenomenon. My subsequent research over the next few years was first reported in a paper for the IJF [43]. This focused on forecasting based on continuous-time dynamic models of the TRF-GTA relationship and showed that a relatively simple continuous-time (CTF) model was able to outperform the large climate models⁵ for short to medium term forecasting (see sub-section 3.3), particularly in relation to the leveling episode.

The model used for forecasting in the above paper was developed with forecasting as its primary objective. While it can be interpreted in mechanistic terms

⁵With the grateful assistance of Professor Geoff Allen, who kindly supplied the climate model data used in the comparison: see figure 11 of the paper.

and provides information on climate parameters, such as *Equilibrium Climate Sensitivity* (CS) (see later), it was not intended for this purpose and employed the DHR algorithm (see Appendix A) to model and forecast an interesting, pentadecadal, oscillatory component that was identified in the data and resulted in the explanation for, and forecasting of, the 2001 leveling episode.

But what might be causing this strange quasi-oscillatory behaviour with its period of around 50 to 60 years? Was it a transient phenomenon? Or could it suggest the presence of a climatically interpretable mechanism that might be explained by some sort of energy transfer or feedback mechanisms within the global climate system? It was questions such as these that led to the next phase in the research that was published recently [45] and which is outlined below. The full details of all the analysis are reported in the associated technical report [50].

3.1. The globally averaged climate data

The data records considered in this paper are the annual, globally averaged climate data, shown in figure 2 for the historical period from 1856 to 2015⁶. These data are derived from the global averaging of measurements carried out by climate scientists and it is assumed here that this global averaging is a legitimate statistical procedure for inferring the changes in the variables at the global level. The *Globally Averaged Temperature Anomaly* (GTA) in figure 2a) represents the changes in the globally averaged surface temperature around a level defined by the background average of the temperature measurements over the period 1951 to 1980. The black dotted line in Figure 2b) shows the changes in the *Total Radiative Forcing* (TRF), which is made up of several components, the most important of which is the CO_2 , shown as the red dotted line. The sharp negative excursions in the TRF which, as we see later, prove useful in establishing the identifiability of the DBM model, are associated with volcanic eruptions.

Figure 2c) shows the *Atlantic Multidecadal Oscillation* (AMO). This is an anomaly signal that represents the pentadecadal ocean heat dynamics for the North Atlantic. It is derived from North Atlantic sea surface temperature patterns, once the trend has been removed, and

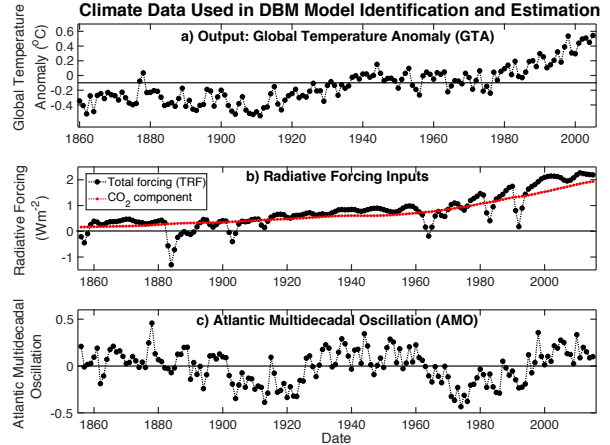


Figure 2: Global Climate Data: a) GTA measurements, from the Carbon Dioxide Information Analysis Center (CDIAC); b) the TRF signal and the CO_2 component of this total signal, from the Potsdam Institute for Climate Impact Research website; c) the AMO series, downloaded from the Physical Sciences Division, Earth System Research Laboratory of NOAA.

was identified by Schlesinger and Ramankutty [26]. In the present analysis, part of the radiative forcing influence on the global temperature response can be isolated and related to the pentadecadal structure present in the AMO. This reveals that the changes represent a component of the globally averaged temperature that is not due to *direct* radiative forcing but, it is surmised, may be due to some of the heat energy arising from the radiative forcing being transferred between the atmosphere and the ocean.

All of the data are affected by uncertainty that arises from various causes, as discussed briefly at the beginning of the IPCC report [25]. In the present paper, it is assumed that this uncertainty results in unexplained disturbance on the GTA series that cannot be explained by the changes in the TRF input and so is modelled as an additive disturbance or ‘noise’, represented by a discrete-time AutoRegressive (AR) model. In other words, the full DBM model is a ‘hybrid’ combination of the continuous-time differential equation model relating the TRF to the GTA, together with a difference equation model for the stochastic disturbance. The presence of this additive stochastic variable, which accounts for only 10% of the variance in the GTA data, is required for optimal stochastic model estimation (see e.g. [40]) and it is reflected in the uncertainty on the estimates of the DBM model parameters, as quantified by the optimization procedures used for model estimation (see Appendix A).

Another important aspect of the data shown in figure

⁶Data download sites: <http://cdiac.ornl.gov/trends/temp/jonescr/jones.html>; <http://www.pik-potsdam.de/~mmalte/rcps/>; <http://www.cgd.ucar.edu/cas/catalog/climind/AMO.html>. Note: The data from these sites were accessed when the present study was initiated and they can change, so the GTA, RTF and AMO data sets used in the present paper can be downloaded as Climate Data.zip from http://captaintoolbox.co.uk/Captain_Toolbox.html/Publication_Downloads.html

2 is that they derive from the measured behaviour of the global system during its ‘normal functioning’. In other words, we have to accept the data in this form, without any possibility of performing planned experiments (see previous section 2). In this situation, the inputs to a dynamic system need to be ‘sufficiently exciting’ for satisfactory statistical identification and estimation of the input-output model [40] and this needs to be evaluated in the statistical identification and estimation process. As we shall see, in this climate context the variations in the TRF caused by volcanic activity appear to provide important excitation in this regard.

3.2. HI-DBM Model Identification and Estimation.

The finally identified CTF model is introduced in equations (A.1)(i) to (iii) of Appendix A. When these are combined they produce the following CTF model:

$$\text{Main System : } x(t) = \frac{b_{10}}{s + a_{11}} u(t) + \frac{b_{20}s}{s^2 + a_{21}s + a_{22}} u(t - \tau) \quad (1)$$

The full details of the model structure identification and associated parameter estimation procedure are described in [50] and it is sufficient here to just discuss the four main stages of this procedure. This also serves to illustrate why I emphasize, in the Introductory section 1, that DBM modeling, unlike ‘black box’ modeling, is not a pre-defined methodology used in a similar way, each time it is applied to a new dynamic system. Rather it is an ‘art and craft’ that requires careful and possibly novel data processing and modeling procedures *if the resulting model is to achieve all of its specified objectives*. Although this means that the data-based modeling process can, at times, be more lengthy, I would maintain that such a careful and rigorous modeling strategy is required in all areas of science, where accuracy is essential and the possibility of inferential errors needs to be minimized.

1. Initial model identification

The first step in the modeling is to consider the identification and estimation of a model between TRF and GTA. The simplest initial approach to such model structure identification [47] is to exploit the consistency power of the *Simplified Refined Instrumental Variable* (SRIVC) estimation algorithm and use the rvcbjid model structure identification routine in the CAPTAIN Toolbox. The hybrid model obtained in this manner

is presented below in the decomposed form shown by equations (i) to (iii):

$$\begin{aligned} x(t) &= x_1(t) + x_i(t), \text{ where,} \\ x_1(t) &= \frac{b_{10}s^3 + b_{11}s^2 + b_{12}s + b_{13}}{s^3 + a_{11}s^2 + a_{12}s + a_{13}} u(t) \quad (i) \\ x_i(t) &= \frac{b_{20}s^3 + b_{21}s^2 + b_{22}s + b_{23}}{s^3 + a_{21}s^2 + a_{22}s + a_{23}} u_{IC} \quad (ii) \\ y(k) &= x(k) + \xi(k) \quad (iii) \end{aligned} \quad (2)$$

Here, the deterministic model output, $x(t)$, is defined as the sum of two variables $x_1(t)$ and $x_i(t)$, where $x_1(t)$ is the output of the main CTF in (i), while $x_i(t)$ is the output of the CTF equation (ii) introduced to allow for the presence of unknown initial conditions on the data. Here, u_{IC} is constant input to this equation which the same size as $x(t)$ and is set to unity over the whole observational interval. The way in which this estimates the effects of such initial conditions is based on Laplace transform theory and is explained briefly in Appendix B. The model is completed by equation (iii), which is the annually sampled output observation $y(k)$ at the k th sampling instant. This is the sum of $x(t) = x_1(t) + x_i(t)$, defined at the same k th sampling instant by $x(k) = x_1(k) + x_i(k)$, and the noise affecting this observation, $\xi(k)$.

Having identified the main model structure, an AR(2) model of the following form is identified for $\xi(k)$:

$$\begin{aligned} \xi(k) &= \frac{1}{1 + c_1 z^{-1} + c_2 z^{-2}} + e(k); \quad (iv) \\ e(k) &= \mathcal{N}(0, \sigma^2) \end{aligned} \quad (3)$$

The full stochastic model (i) to (iv) is then re-estimated optimally in its hybrid form, including the discrete-time noise model, using the rvcbjid routine. And finally, the residual white noise $e(k)$ is checked to see that it satisfies the required serial and cross correlation tests.

The top panel in figure 3 (see next page) compares the resulting simulated model output $\hat{x}(k)$ with the measured GTA $y(k)$. As we see, model represents the data quite well, with $\hat{x}(k)$ explaining 90% of the $y(k)$ output variance: i.e. the *Coefficient of Determination* $R_T^2 = 0.90$, where this is based on the variance of the ‘output error’ $\hat{\xi}(k) = y(k) - \hat{x}(k)$.

The lower panel in the figure shows the two constituent responses $\hat{x}_1(k)$ and $\hat{x}_i(k)$. These are immediately very revealing, showing that the initial condition response is dominated by a very low-damped sinusoidal signal which accounts for low level cyclical behaviour that has now been exposed clearly in the GTA response.

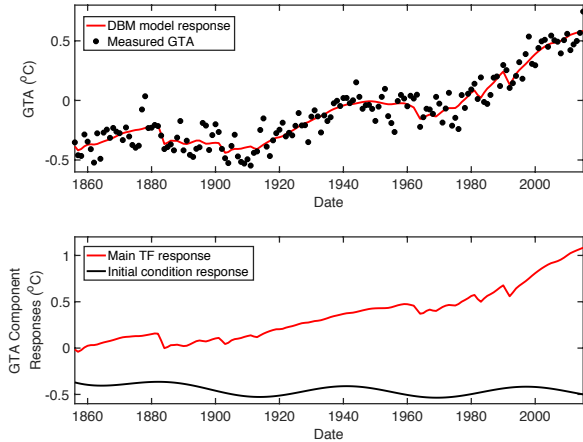


Figure 3: The upper panel compares the output of the initial model with the GTA data and the components of this response are shown in the lower panel.

2. Initial Parametric Evaluation

Each CTF in the initially identified model (2) in stage 1 can be decomposed, using the Matlab routine `residues`, into first order and second order CTFs. In addition, application of ‘dispersion analysis’ (see Liaw [15]), using the `liawc` routine in CAPTAIN⁷, shows that the first order mode in the first CTF represents 99.9% ‘relative power’ (see [15]), while the oscillatory mode in the second CTF has 98.8% relative power. This is supported by the step response and Bode (Gain and phase against frequency) diagrams, which confirm this decomposition.

Based on this decomposition, the dominant first order mode, in the first equation, has an estimated time constant $\hat{T} = 21.4$ years; while the the second order oscillatory mode, in the second equation, has an estimated period $\hat{P}_n = 56.1$ years. In addition, an estimate \hat{CS} of the climate sensitivity CS can be obtained, based on the directly estimated model parameters. Here, $CS = 3.7 \times G = 2.32^\circ\text{C}$, where $G = 0.625$ is the ‘steady state gain’ (see Appendix A) of the first CTF and 3.7 is the radiative forcing in W/m^2 associated with *doubling the CO₂ level in the atmosphere*.

If point estimates of these derived parameters \hat{CS} , \hat{T} and \hat{P}_n are all that is required, the modeling could stop at this stage. However, the uncertainty in these estimates can be obtained easily using MCS analysis based on the estimated parametric covariance matrix, as shown in Table 1. It is clear from this table that the parametric uncertainty in this initial model is too large, partly because

⁷A continuous-time version of Liaw’s discrete-time algorithm.

Parameter	Estimate	Lower 5% Bound	Upper 95% Bound
\hat{CS} ($^\circ\text{C}$)	2.32	2.05	3.34
\hat{T} (years)	21.4	13.2	72.6
\hat{P}_n (years)	56.1	51.8	63.2

Table 1: MCS results for the Initial DBM Model based on 10,000 random realizations defined by the estimated error covariance matrix.

the model is of quite a high order: 14 parameters in the two CTFs of equations (2)(i) and (ii), compared with the final, much more parametrically efficient 5 parameter model (4) considered below in stage 5. In addition to this relatively high order, the main problem with the model is that the interesting sinusoidal behaviour is associated with the initial condition response $x_i(t)$. It would be preferable is this was integrated with the main CTF in some manner, so that it can be interpreted in more physically meaningful terms.

3. Model Order Reduction

Based on the decomposition of the TFs in stage 2, it best to assume that these CTFs are of the identified lower dimensional forms, with appropriate order polynomials. The model is re-estimated in this reduced order form using the `rvcdd` routine in CAPTAIN or the `ttest` routine in Matlab⁸. The resulting continuous-time model has two different order CTFs characterized by only 8 parameters and yet it explains the data as well as the initial 14 parameter model, with $R_T^2 = 0.90$. On the other hand, two of the numerator polynomial parameters in the second order CTF have very large standard errors. While this is a reasonable model, these questionable uncertainty results, together with the oscillatory mode still being associated with the initial condition response $x_i(t)$, suggest that it should be possible to identify a better model without these deficiencies.

4. Final Model Identification and Estimation

In order to remove the need for the initial condition equation and the additional input u_{IC} required for this, the final identification and estimation of the model is carried using a simulated model in the Matlab ‘Simulink’ software application. This has the advantage that the initial conditions can be introduced directly as parameters in the three integrators of the simu-

⁸The `ttest` routine in Matlab is easier to use and somewhat more reliable, although it does not report a noise model. The final model (4) (see next stage 4.) is slightly simpler than the `ttest` estimated model, with one less parameter, and it includes a noise model.

lated differential equations (The Simulink diagrams are shown in the Appendix of [50]). More importantly, it was found by experimentation that the oscillatory behaviour could be explained using the delayed input TRF signal (denoted by $u(t - \tau)$ in equation (4) below), rather than allowing this to be explained by the initial condition response. This was motivated by noting that the more rapid variations in the TRF series, caused by volcanic activity, appeared to be linked with the oscillatory behaviour if this signal was delayed by about $\tau = 17$ years.

The deterministic equations of the finally optimized Simulink model, presented in CTF form, are as follows,

$$\begin{aligned} x_1(t) &= \frac{b_{10}}{s + a_{11}} u(t) & (i) \\ x_2(t) &= \frac{b_{20}s}{s^2 + a_{21}s + a_{22}} u(t - \tau) & (ii) \\ x(t) &= x_1(t) + x_2(t) & (iii) \end{aligned} \quad (4)$$

where τ is a time delay estimated when the model is optimized *allowing for a fractional delay* (see below). It will be noted that the numerator of the $x_2(t)$ equation is now identified to have only one term, $b_{20}s$, showing that $x_2(t)$ is the *filtered first derivative* of $u(t - \tau)$.

The differential equation equivalent of (4), as used in the Simulink model, takes the form:

$$\begin{aligned} \frac{dx_1(t)}{dt} &= a_{11}x_1(t) + b_{10}u(t) & (i) \\ \frac{d^2x_2(t)}{dt^2} &= a_{21}\frac{dx_2(t)}{dt}s + a_{22}x_2(t) + b_{20}\frac{du(t - \tau)}{dt} & (ii) \\ x(t) &= x_1(t) + x_2(t) & (iii) \end{aligned} \quad (5)$$

This allows the model to be compared directly with the climate models that are normally represented in this form, rather than as CTF models. The full DBM model is then completed by the following discrete-time equation for the measured GTA, $y(k)$,

$$\begin{aligned} y(k) &= x(k) + \xi(k) \\ \xi(k) &= \frac{1}{1 - c_1 z^{-1}} e(k) \quad e(k) = \mathcal{N}(0, \sigma^2) \end{aligned} \quad (6)$$

This final model is now identified with only 5 parameters in the continuous-time model, plus the 3 initial conditions on the integrators.

The model parameters are estimated using the Matlab optimization routine lsqnonlin, which is programmed to repeatedly call the Simulink model, add a discrete-time equation for the noise model, and minimize the sums of squares of the resulting residual series $e(k)$. This is referred to as ‘prediction error minimization’ in the

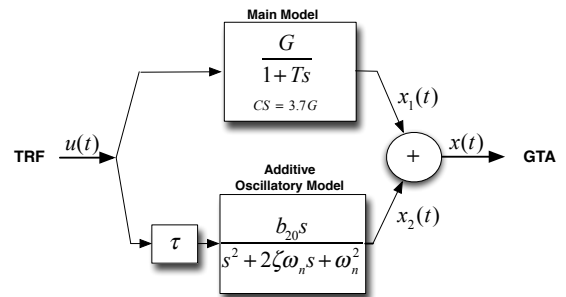
systems and control literature (see e.g. [40]). Initially, the starting estimates for this optimization were selected from the estimated parameters of the model obtained in stage 3.

On convergence, the model yields a good explanation of the data ($R_T^2 = 0.90$) and the resulting parameter estimates are as follows, where the standard errors are shown in parentheses:

$$\begin{aligned} \hat{a}_{11} &= 0.0518(0.005); \hat{b}_{10} = 0.0320(0.003); \\ \hat{b}_{20} &= 0.0067(0.006); \hat{a}_{21} = 0.0082(0.013); \\ \hat{a}_{22} &= 0.0129(0.001) \hat{c}_1 = -0.220(0.078); \hat{\sigma}^2 = 0.008; \\ \hat{I}C1 &= -0.32(0.049); \hat{I}C2 = 0; \hat{I}C3 = -0.031(0.036); \end{aligned}$$

The estimate of the time delay $\hat{\tau} = 17.5(4.4)$ years shows that the data are explained better if this is ‘fractional’ [7] and not an integral sum of sampling intervals, which is normally assumed in most discrete-time models. As required, the model residual series $e(k)$ is serially uncorrelated and uncorrelated with the TRF input.

Figure 4 is the ‘block diagram’ of this model, as shown in figure A.5 of the Appendix but repeated here for convenience. It shows that the model can be considered as a parallel connection of the two constituent CTF models. It also reveals the values of the *derived parameters*: Steady-State Gain, $G = \frac{b_{11}}{a_{11}}$; Time Constant, $T = \frac{1}{a_{11}}$; Natural Frequency, $\omega_n = \sqrt{a_{22}}$; and Damping Ratio, $\zeta = \frac{a_{21}}{2\sqrt{a_{22}}}$. These immediately provide information about the dynamic nature of the system *without having to resort to the solution of the underlying differential equation*.



$$\begin{aligned} G &= 0.618; T = 19.3 \text{ y}; CS = 2.29; b_{20} = 0.0067; \tau = 17.5 \text{ y} \\ \omega_n &= 0.0181 \text{ c/y; (period } 55.3 \text{ y}); \zeta = 0.036 \end{aligned}$$

Figure 4: Block diagram of the final DBM model.

Finally, it is worth noting that discrete-time model identification does not work well at this annual sampling rate: e.g. if such a model is estimated using the annual sampled data, the explanation of the data is reduced

and the model does not reveal the oscillatory mode. It is possible to identify a marginally acceptable 4th order discrete-time model if the data are sampled more coarsely, with a sampling interval of 3 years (i.e. sample size reduced to 54). This model has an oscillatory mode of 63 years but this is quite highly damped (damping ratio 0.7) and the estimated CS is low at 1.64°C . These mixed results, combined with the higher parametric uncertainty caused by both the reduced sample size and the higher order model, means that the model has to be rejected as unsatisfactory when compared with the lower order, differential equation model (5), which is very much better defined in statistical terms.

4. Mechanistic Interpretation

Let us consider first the equation (5)(i) relating the total radiative forcing to the changes in global average surface temperature. The following simple, conceptual, energy-balance model of the climate system temperature response to changes in radiative forcing has been suggested many times in the climate literature (see e.g. [3]):

$$C \frac{d\Delta T(t)}{dt} = F(t) - \lambda \Delta T(t) \quad (7)$$

Here, C is a constant *Effective Heat Capacity* (EHC) per unit area; $\Delta T(t)$ is the global-mean surface temperature; $F(t)$ is the TRF; and the constant λ represents ‘feedback processes’ within the global climate system. This equation can be compared directly with (5)(i) and we see that $C = 1/b_{10} = 31.2 \text{ Wym}^{-2}\text{K}^{-1}$ and $\lambda = Ca_{11}/b_{10} = 1.618 \text{ Wm}^{-2}\text{K}^{-1}$. In the context of the present paper, the steady state gain $G = \frac{1}{\lambda} = 0.618$ and the time constant $T = \frac{C}{\lambda} = 19.3$ years, which Andrews and Allen [3] call the *Feedback Response Time* (FRT).

One advantage of the present analysis, in relation to that of Andrews and Allen [3], is that we are able to evaluate the uncertainty in all the derived parameter estimates using MCS analysis based on the estimated parametric covariance matrix. The results from this analysis are shown in Table 2 below:

Parameter (units)	Estimate	Lower 5% Bound	Upper 95% Bound
$\hat{ECS} (^{\circ}\text{C})$	2.29	2.11	2.49
$\hat{T} (\text{y})$	19.3	16.5	23.3
$\hat{P}_n (\text{y})$	55.3	51.60	60.0
$\hat{\lambda} (\text{Wm}^{-2}\text{K}^{-1})$	1.62	1.49	1.75
$\hat{C} (\text{Wym}^{-2}\text{K}^{-1})$	31.2	26.9	37.3

Table 2: MCS results for the Final DBM Model based on 10,000 random realizations defined by the estimated error covariance matrix .

All of these derived parameters have a physical interpretation and are utilized in climate research. They can be compared with those in Table 1 of Randall *et al* [25], as obtained from the analysis of 18 AOGCMs used by the IPCC. Based on this table, the mean and two standard deviations (95% bounds) for the ECS and T , respectively, are $2.95(1.92) ^{\circ}\text{C}$; and $30.3(17.4)$ years, which can be compared with our DBM model results which, in the same format, are $2.29(0.74) ^{\circ}\text{C}$ and $18.4(5.8)$ years. The estimate of EHC, $\hat{C} = 31.2 \text{ Wym}^{-2}\text{K}^{-1}$, with a 95 percentile range of 26.9 and 37.3, is in reasonable agreement with Knutti *et al* [12], who provide an estimated EHC of $24 \pm 11 \text{ Wym}^{-2}\text{K}^{-1}$, based on their analysis of seventeen CMIP3 GCM models.

While the interpretation of equation (5) is straightforward, (5)(ii) presents a more difficult problem because nothing like this has appeared previously in the climate literature. As we see from Table 2, the oscillatory state $x_2(t)$ has an estimated period of 55.3 years, with a 95 percentile range between 51.6 and 60 years; while the damping ratio is quite close to zero at $\zeta = 0.036$ (so, without any changes in the input $u(t - \tau)$, the oscillations will decay slowly in amplitude until they die out: see Appendix A. Most significantly in climatic terms, however, the recession periods of this oscillation coincide with and help to explain the climate shifts (‘pauses’ or ‘levelling’) in the generally upward trend of the GTA, as shown in figure 5 and the forecasting results in [43].

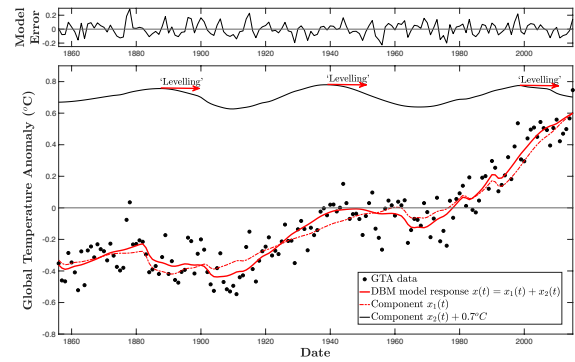


Figure 5: The output of the final DBM model (red full line) compared with the GTA data. Also shown are the component states $x_1(t)$ (red dash-dot line) and $x_2(t)$ (black line), which is raised by 0.7°C for clarity.

The potential importance of quasi-cyclic behaviour with a period of around 50-70 years has been known for some time. For example, Schlesinger and Ramankutty [26] applied singular spectrum analysis to four global-mean temperature records and identified a temperature

oscillation with a period of 65-70 years. They conclude that this is the statistical result of 50-88 year oscillations for the North Atlantic Ocean and its bounding Northern Hemisphere continents. Moreover, this AMO variable, as well as other multi-decadal oscillatory phenomena measured by climate scientists, could be redolent of complex internal energy exchange mechanisms that are giving rise to significant quasi-cyclic behaviour in the ocean-atmosphere system. These may be related to the oscillatory state variable $x_2(t)$ in the DBM model (5) and its CTF equivalent (4).

Some additional insight into the nature of the $x_2(t)$ model can be obtained by decomposing the second order CTF model (4)(ii) into the feedback connection of two first order CTF components. The state space equa-

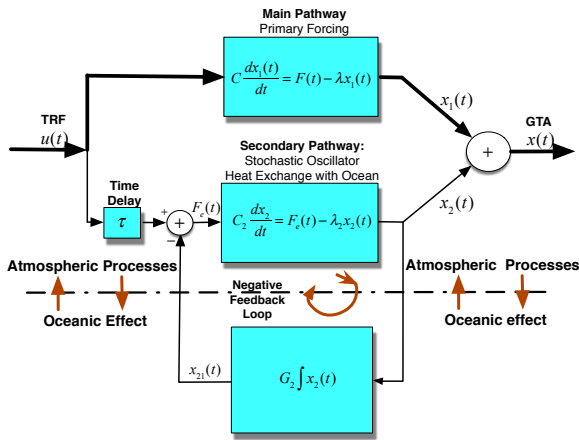


Figure 6: Climatic Interpretation of the DBM Model.

tions of this decomposed model can be written as follows

$$\begin{aligned} C_2 \frac{dx_2}{dt} &= -\lambda_2 x_2(t) + F_e(t) \\ \frac{dx_{21}}{dt} &= G_2 x_2(t) \end{aligned} \quad (8)$$

where $x_{21}(t)$ is the ‘feedback path’ variable and $F_e = u(t - \tau) - x_{21}(t)$ is the difference between the delayed incoming TRF input and $x_{21}(t)$, which provides the input to the energy balance equation in the forward path.

This is shown diagrammatically in the lower part of figure 6, which is a block diagram of the whole DBM model with its two ‘pathways’ defined by the main two equations of the model. The lower pathway shows the negative feedback system representing the equations (8), where the feedback path consists of a simple integrator with gain G_2 that accumulates the changes in the $x_2(t)$ component of the GTA. The estimated parameters in this feedback model are $C_2 = 148 \text{ Wym}^{-2} \text{K}^{-1}$; $\lambda_2 = 1.22 \text{ Wm}^{-2} \text{K}^{-1}$ and $G_2 = 1.913$; while the decomposed

model in CTF form has estimates of the forward path gain $G_2 = 0.821$ and time constant $T_2 = 121.9$ years. Note that, although these estimates are not as well defined statistically as those in the main constituent model A.4(i) for $x_1(t)$, the feedback decomposition itself is very well defined.

The overall effect of this negative feedback mechanism is to create the oscillatory mode of behaviour that is so important in explaining the subtle oscillatory ‘quasi-cycle’ variations observed in the GTA. In other words, the combination of the gains and time constants in the two boxes is creating some form of heat energy exchange that promotes the oscillatory nature of the response. The presence of the integrator in the feedback path suggests that this feedback part of the system relates to mixing processes that are very long term. This is consistent with slow transport processes that occur slowly in the global oceanic system, which is accumulating the effects of the changes in the globally averaged temperature.

In this way, the interchange of energy between the atmosphere and the ocean, and vice-versa, can be considered as a physical process that, over the past 160 years, has helped to sustain the oscillatory movements in $x_2(t)$ and so caused fairly regular, periodic changes in the GTA, one of which led to the leveling in the GTA after the start of the new Millennium. It must be emphasized, however, that while the structure of this decomposition is well defined, the parameters that characterize this structure are quite uncertain, following from the uncertainty in the parameters of equation (5)(ii). As a result, the values of the parameters in the decomposed system, and any interpretation of them, must be considered with some circumspection.

Finally, in this mechanistic interpretation of the DBM model, it is necessary explore the possibility of relating the oscillatory state $x_2(t)$ and the low frequency dynamic behaviour represented by the AMO series and its quasi-periodic oscillations. Schlesinger and Ramanukutty [26] suggest that there are three possible sources for the AMO signal: (i) random forcing, such as by white noise evoking a coloured signal response; (ii) external oscillatory forcing arising from variations in the solar constant; and (iii) an internal oscillation of the atmosphere-ocean system. They reject the first two possibilities and conclude that the most probable cause of this oscillation is an inherent internal oscillation of the atmospheric-ocean system. This seems a reasonable argument and so it makes sense to consider how the AMO oscillations can be modeled in a way that links them with the internal oscillatory state $x_2(t)$ in the model (5).

The full details of this analysis are given in [50], where a separate second order CTF model is identified and estimated between $x_2(t)$ and the AMO series. Figure 7 shows the stochastic simulation results for the re-

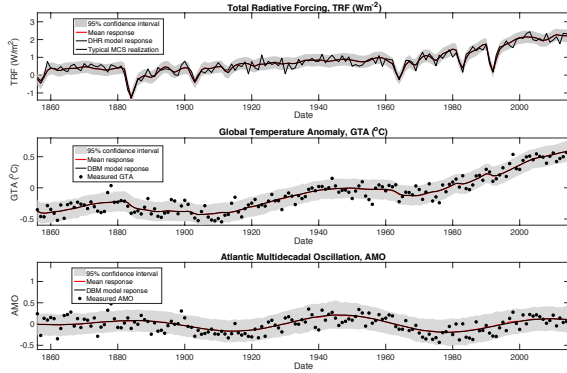


Figure 7: Stochastic simulation results from the final DBM model including an integrated AMO state.

sulting full DBM model, as obtained by combining this AMO CTF model with the model (4). The TRF, which is the only forcing input to the model, is plotted in the top panel. This was modeled using the DHR routine and the red line shows the DHR model output, with the associated 95% confidence bounds shown in grey. Below this are plots of the deterministic model outputs and the 95% bounds on these obtained from the MCS analysis. The model GTA response is compared with the measured GTA in the middle plot; and the modeled AMO response is compared with the measured AMO series in the lower panel.

3.3. Application of the DBM model

In addition to its use in explaining the globally averaged data and providing a physically meaningful explanation of its implications in climatic terms, the DBM model (4) can also be used in various application contexts: forecasting; scenario investigation; and possibly in the management of carbon emissions using the automatic control methodology available in CAPTAIN. Once again, these are all discussed in [50] and only the results of such analysis in the first two cases will be presented here using the four plots shown in figures 8 to 11.

Figure 8 shows how the DHR forecasts of the TRF and its uncertainty bounds, as shown in the top panel, are used by the DBM model to forecast the globally averaged temperature anomaly (GTA) for a long time into the future. The TRF forecasting results in the top panel were obtained from a standard application of dhr routine

in CAPTAIN (i.e. equation (A.8) with just the $T(k)$ and $W(k)$ components). Not surprisingly, the almost random effects of volcanic activity are not captured by the DHR model so, for illustrative purposes, some perturbations have been added to mimic this behaviour into the future, based on the past activity. The dhr computed uncertainty associated with the TRF input is then amplified by the uncertainty in the DBM model as this TRF input is processed by the model, so that the total uncertainty on the GTA (light grey) is very large. On the other hand, the uncertainty due to that in the DBM model alone (dark grey) is relatively small. This is because all the parameters in the main equation (4)(i) are estimated so well and, as a result, these bounds are able to encompass the latest GTA measurements (red dots).

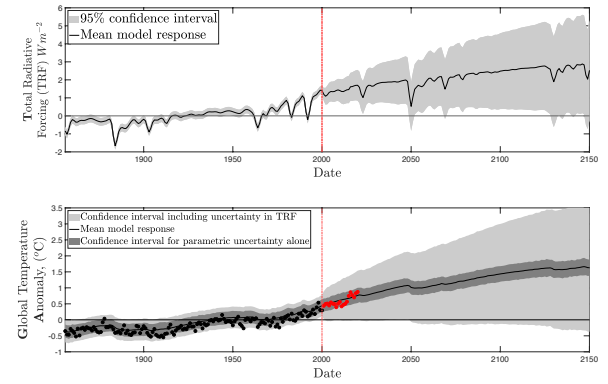


Figure 8: Illustrative example of forecasting using the DBM model from a forecasting origin (FO) in 2000.

These forecasting results are not too bad considering that the model was not intended for use in the manner. A better formulation of the model for forecasting purposes is that described in Young [43], where the oscillatory mode is modeled by the time variable parameter DHR model, so allowing for continual adaption at every sample. This forecasts the leveling after 2000 much better, as shown in figure 9, where we see that the forecasts are also a considerable improvement on the AOGCM model forecasts⁹, which completely fail to predict the leveling episode despite their size and complexity.

A more reasonable but related application of the DBM model is for ‘scenario’ analysis, where it is used to assess what might happen to the GTA under different future TRF scenarios. Such ‘what-if’ analysis is very popular with climate scientists but their extremely large, computationally intensive, simulation models are ill-suited to the task and so smaller, computationally

⁹Data kindly supplied by Professor Geoff Allen.

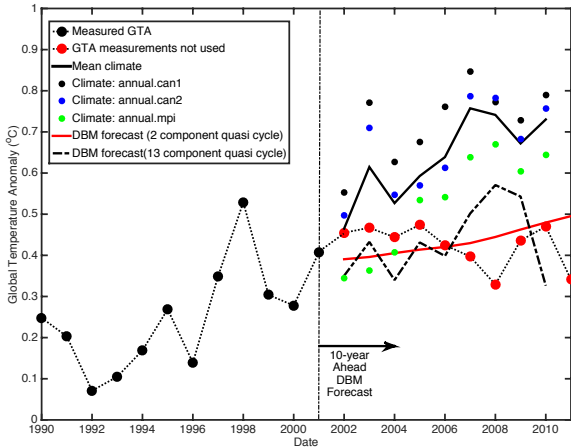


Figure 9: Comparison of DBM model forecasts and typical AOGCM climate model projections.

simple but still high order ‘emulation’ models have been used for this purpose: for instance, a typical implementation of the well-known MAGICC emulation model (e.g [17, 43]) is 80th order. The DBM model, on the other hand, is only 3rd order and computationally very fast, so that the scenarios and their associated uncertainty bounds are easy to compute over an extended scenario period.

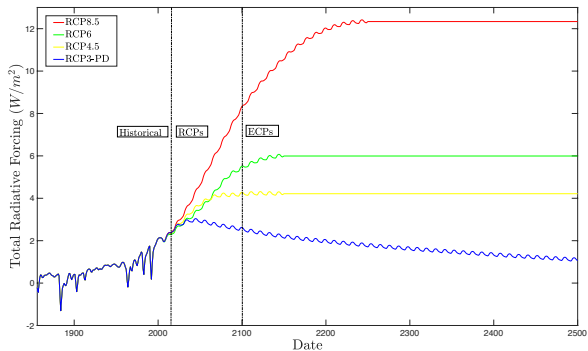


Figure 10: The four *Representative Carbon Pathway* (RCP) scenarios used for the analysis shown in figure 11.

Figures 10 is a plot of four future *Representative Carbon Pathway* (RCP) scenarios prepared by the task group ‘RCP Concentrations Calculation and Data’ in the preparation of the IPCC Fifth Assessment Report [18]. The four scenarios are defined by four different hypotheses about the future behaviour of the TRF from 2015 to 2500¹⁰: (i) taking no action to reduce future

¹⁰source: <http://www.pik-potsdam.de/~mmalte/rcps/>

emissions (‘Business as Usual’); (ii) and (iii) reduction in the emissions based on current pledges by Governments (‘Current Pledges’); and finally (iv), one optimistic scenario where reductions are much greater than the current pledges (‘Optimistic Reductions’). Each of these is totally deterministic, without any assumptions about its uncertainty into the future, after the historical period.

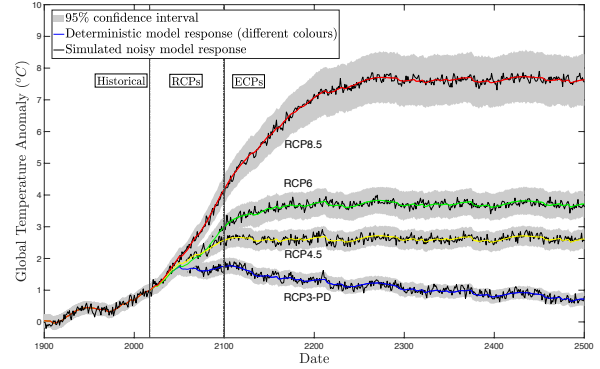


Figure 11: DBM model responses to the four scenarios in figure 10.

Figure 11 is the plot of the DBM model-based GTA outcomes using these TRF scenarios as inputs. Here, as in the forecasting case, the future perturbations in the TRF are based on the volcanically-related perturbations that occurred over the historical period. These are added to the scenarios in figure 10 over the future period, so that the oscillatory mode is activated over the associated future responses. This leads to the repeated perturbations in the temperature and fairly wide confidence bounds which are based only on the uncertainty in the model parameters and measurement noise. As in the forecasting example above, they would be much larger if the considerable uncertainty associated with the future TRF was also taken into account. These scenario simulations involve MCS analysis based on 1000 realizations (the simulated noisy model response is shown as a black line in each case) but because the model is so small, the computational cost is very small. Of course, such an MCS exercise would be very difficult, if not impossible, with the large climate models.

4. The Monitoring and Forecasting the Progression of the COVID-19 Epidemic

Given the extensive description of the global climate example in the previous section, this second practical application, which is concerned with the COVID-19 pandemic, will be discussed in much less detail, presenting only the main results obtained in the study and

concentrating mostly on some of plots that illustrate these results. For those readers interested in this research, it has been published recently [51] and more details can be found there and in an associated technical note [44]. It is primarily concerned with the monitoring of the COVID-19 epidemic in the UK, Italy, Germany and the USA; and forecasting of the COVID-19 epidemic in the UK. Research on nonlinear modeling based on SDP analysis is included in the published paper but will not be discussed here.

4.1. Monitoring

In the past, epidemics have been monitored by various statistical and model metrics, such as evaluation of the effective reproduction number, $R(t)$. However, $R(t)$ can be difficult and time consuming to compute. A much simpler approach to monitoring an epidemic is described in [51]. Here, the COVID-19 epidemic is considered as a classical, noisy, dynamic system whose progress can be monitored by two new metrics: one based on optimally smoothed estimation of the epidemic *rate of change* (RC); and the other on a related state-dependent *response rate parameter* (RP) which will not be discussed in the present paper. These metrics are evaluated and discussed in relation to the daily confirmed cases of COVID-19 and the daily deaths arising from these in the UK and Italy¹¹. Of course, these metrics in no way replace the $R(t)$ metric. Rather they provide much more rapidly computable, adaptive measures that reveal the underlying progress of the epidemic and, as we shall see, help to predict how the epidemic may develop in the near future.

A typical example of the epidemic data used in the evaluation of the RC and RP metrics is shown in figure 2, where the UK and Italian data are plotted in red and black colours, respectively. Note that the UK data, in particular, are characterized by a changing weekly cycle caused by the methods of data collection and delays that occur in this operation, particularly at weekends. In this figure, the upper panel shows the cumulative series, while the lower panel shows the daily deaths. The UK epidemic started 15 days after the Italian epidemic so the UK series has been shifted by 15 days to illustrate the similarity in the series.

Although there is a weekly cycle in the Italian series, it is most pronounced in the UK series and, clearly, it

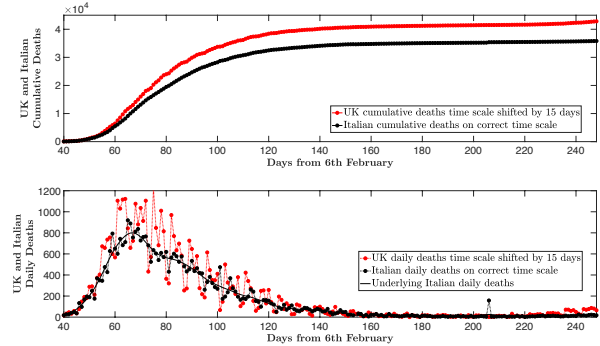


Figure 12: Cumulative and daily UK and Italian Deaths data.

needs to be accounted for in the data analysis. Consequently, both metrics are based on DHR estimation, using the `dhr` routine in CAPTAIN. In this application, the UC model takes the reduced form (see Appendix A):

$$\begin{aligned} y(k) &= x(k) + W(k) + e(k) \\ e(k) &= \mathcal{N}(0, \sigma^2) \end{aligned} \quad (9)$$

where $y(k)$ is the daily deaths series and the DHR algorithm decomposes this series, at sampling instant k , where $k = 1, 2, \dots, N$ and N is the sample size, into two unobserved components: $W(k)$, accounting for the weekly cyclical behaviour; and $x(k)$ (replacing $T(k)$ in equation (A.8) of Appendix A) modeling the underlying changes in the series being considered.

The estimated $x(k)$ signal in the UC model provides an optimally smoothed estimate of the changes in $y(k)$ after the weekly cycle and noise have been removed. Most importantly for the purposes of the present paper, the DHR analysis also yields an optimal estimate of the continuous-time temporal rate of change $\frac{dx(t)}{dt}(k)$, which defines the RC metric at the k th sampling instant. The estimation of this unobserved component model and the resulting RC metric is computationally very rapid and provides a virtually instantaneous estimate of how RC is changing every day, as soon as the latest update in the number of deaths is received.

An example of this RC estimation is shown in figure 13, which provides an illustration of how the metric changes over the 150 day period and how these changes can be interpreted. Here, RC is plotted as a red line with its estimated uncertainty shown in light grey. Two regions are marked in light colours: a ‘Danger Zone’ in light red where $RC > 0$ and the death numbers are increasing in some manner; and a ‘Safe Zone’ in light green, where $RC < 0$ and the numbers are decreasing. These results are obtained from analysis of the measured UK daily deaths data, standardized to measure

¹¹Most of the COVID-19 data used in this paper were downloaded from the GitHub Web Site at https://github.com/CSSEGISandData/COVID-19/tree/master/csse_covid_19_data/csse_covid_19_time_series.

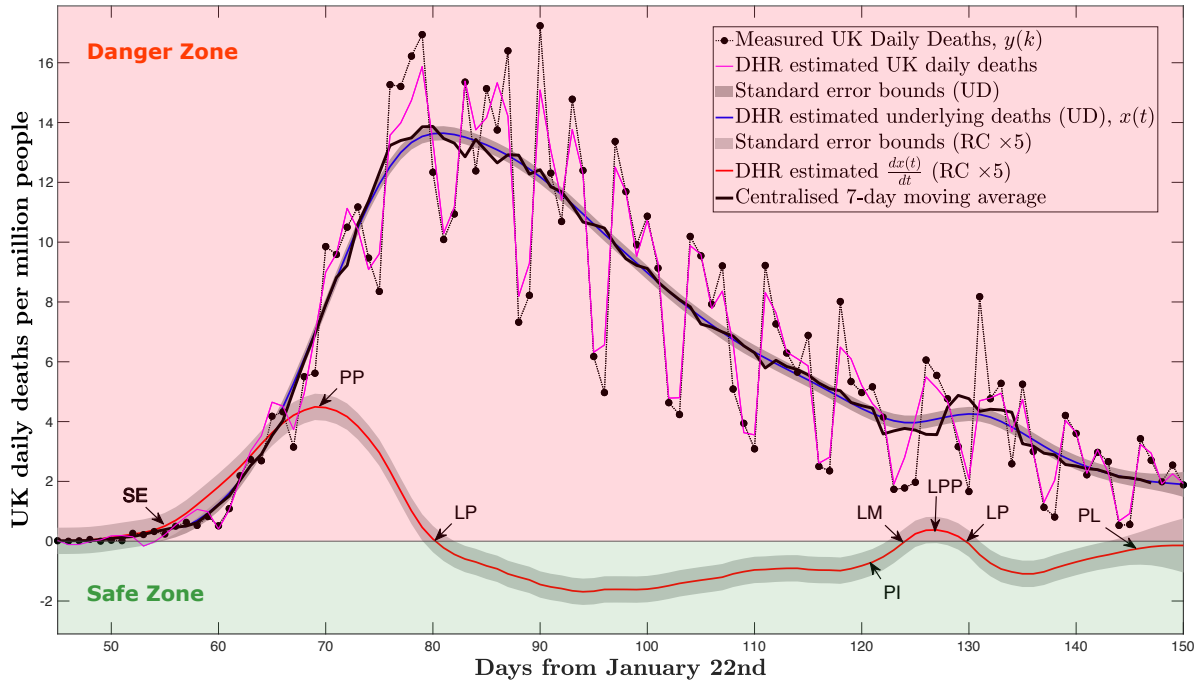


Figure 13: Progress of the UK epidemic monitored by the RC metric.

the deaths per million people and plotted as black dots. Such standardization is used for all of the results presented subsequently and, in this case, the UK population is rounded to 68 million.

The magenta line is the full estimate from the UC model: its uncertainty bounds are not shown in order to simplify the plot. The blue line with associated dark grey uncertainty bounds, is the DHR estimate of the underlying daily deaths $x(k)$, which is smooth and very effectively corrected for the cyclical factors. Figure 13 also shows, as a thick black line, the well known centralised 7-day moving average, which appears to be the preferred measure of the underlying behaviour in epidemiology and has been shown increasingly in the material published by the UK Government¹². It is taking the weekly cycle into account in a much cruder manner than DHR, so it is more volatile and, because of the way it is computed, it cannot be estimated at the beginning and end of the series.

The various letters on figure 13 point to interesting times as the epidemic proceeded and these are discussed fully in [51]. For example, PP shows where RC has detected the maximum rate of change before the epidemic starts to move towards its peak, thus predicting that the

peak is being approached; while LP shows the location of the peak, defined as RC crosses zero at sample 80 on April 11th.

Finally, figure 14 shows what has happened to the RC metric when applied to the deaths (right panel) and confirmed cases (left panel) in the UK epidemic for the whole time up to a forecasting origin FO on September 27th 2020. After the section of the epidemic shown in figure 13, the deaths and confirmed cases continued to drop and the deaths appeared to be leveling out, signaling an end to the epidemic and giving rise to a premature relaxation, by the overly-optimistic UK Government, in the restrictions that had applied over the lock-down period. However, the RC metric for the confirmed cases moved into the danger zone at the location shown by the red arrow in the left-hand panel and, two days later, the confirmed case started to rise sharply, a trend that has continued, with only small down-turns from time-to-time, until the end of the plot.

On the other hand, the number of deaths continued to drop with the RC metric hovering around zero. On August 31st, however, at the location shown by the red arrow in the right-hand panel, there was an ominous, sustained rise of RC into the danger zone, as shown in the enlarged inset on the plot. This heralded a subsequent initial rise in deaths that soon produces a second wave of the epidemic. This is consistent with the very large rise

¹²<https://coronavirus.data.gov.uk/#category=nations&map=rate&area=n92000002>

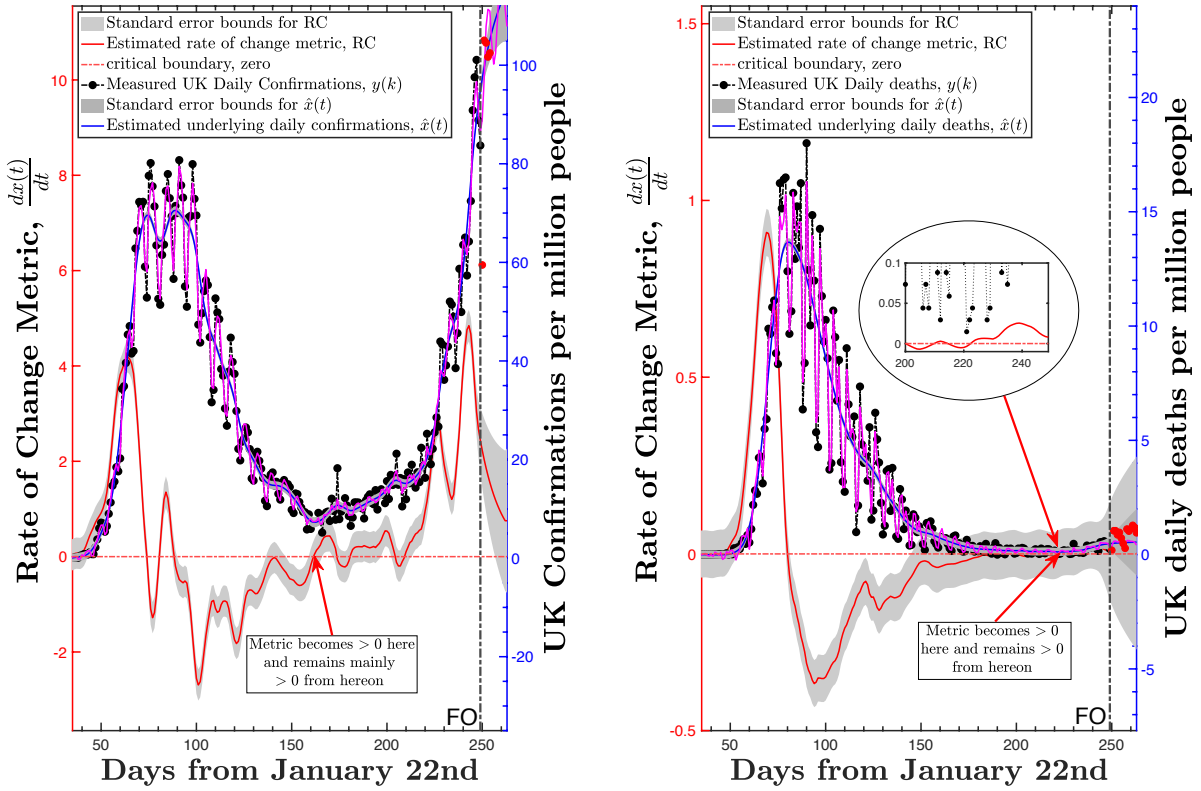


Figure 14: Rate of Change metric applied to UK Confirmed and Deaths data.

in confirmed cases, shown in the left-hand panel, and an associated rise in hospital admissions (not shown). The fact that it took much longer than expected for the death numbers to increase when the confirmed cases were rising so sharply has been put down to the inaccuracy of the badly implemented and managed test-and-trace system that was ‘out-sourced’ to a private company by the UK Government. Also, a lot of the confirmed cases were amongst younger people who did not develop dangerous symptoms that required hospitalization¹³

4.2. Forecasting

Figure 12 has shown the similarity of the Italian and UK epidemic behaviour in the first wave of the epidemic, but with the UK having larger numbers of confirmations and deaths (partly consistent with the slightly larger UK population: 68 cf 60.5 million, a ratio of 1.124). Given this similarity, it is interesting, over this first wave, to consider relating the two epidemics in

some manner. The simplest approach is to estimate a *Dynamic Linear Regression* (DLR) model of the following form between the cumulative death numbers:

$$y_c(k) = \beta_0(k) + \beta_1(k)z_c(k) + e(k) \quad (10)$$

where $y_c(k)$ and $z_c(k)$ are, respectively the cumulative deaths in the UK and Italy; while $\beta_0(k), \beta_1(k)$ are TVPs modeled as GRW processes (see Appendix A).

This DLR model could be used directly for modeling and forecasting the daily death series in the UK by exploiting the 15 day lead provided by the Italian data to achieve 15-day-ahead forecasting. However, the same objective can also be achieved, with much better accuracy, if a hybrid continuous-time model, of the general kind used previously in section 3, is applied to the underlying dynamic relationship between the two series. This model is of the following form:

$$x(t) = \frac{B(s)}{A(s)}u(t - \tau) \quad (i)$$

$$y(k) = x(k) + W(k) + \frac{D(z^{-1})}{C(z^{-1})}e(k) \quad (ii) \quad (11)$$

$$e(k) = \mathcal{N}(0, \sigma^2) \quad (iii)$$

¹³Other monitoring examples, using both the RC and RP metrics applied to UK, Italian German and USA data are given in [51] and [44].

where $u(t-\tau)$ represents the underlying behaviour of the Italian series, delayed by $\tau = 15$ days. Further details of the above model and its estimation are given in the paper [51].

A typical example of the forecasting results obtained using the model (11) is illustrated by the three plots in figure 15, which show 15-day-ahead forecasts made

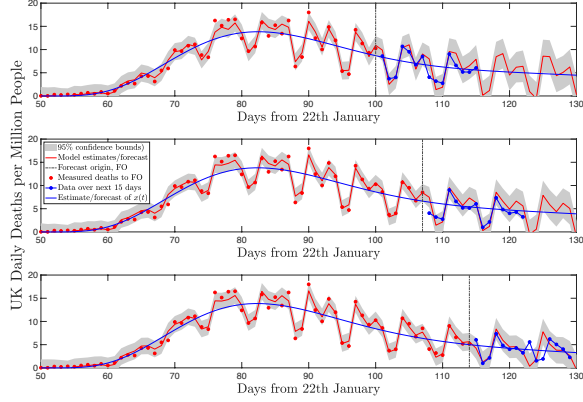


Figure 15: Adaptive, rolling estimation and forecasting results for UK daily death numbers during the COVI-19 epidemic.

from forecast origin locations spaced at 7 day intervals. A 7-day-ahead forecast is probably the most useful in practical terms because the forecast begins to deteriorate a little after this. Given the changing nature of the weekly cycle, the forecasting performances illustrated by this figure are quite reasonable and, together with the RC metric, provide a good idea of what to expect over the next two weeks of the epidemic, as required for management and decision making during an epidemic such as COVID-19. It is felt that such simply updated forecasts could enhance the information gained at present from the traditional epidemic models, particularly as the DHR component accounts so well for the changing weekly cycle.

Finally, it is important to note that the transfer function modeling approach discussed in this section can be used in any situation where there are sufficient data available for a linear CTF relationship to be identified between the measured time series. One interesting illustration of this approach is based on the estimated CTF relationship between the data on the number of COVID-19 patients in UK hospitals¹⁴ and the subsequent COVID-19 deaths. This example is discussed fully in the technical note [44] but figure 16 shows an

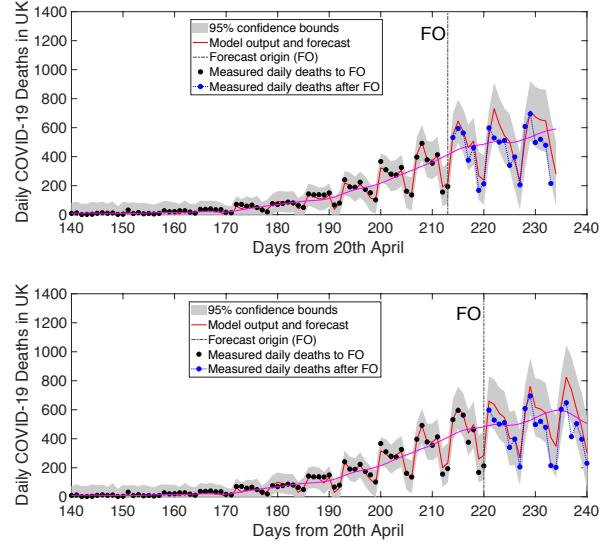


Figure 16: Two examples of the UK COVID-19 forecasting results based on the number of COVID-19 patients in UK hospitals.

example of three-week-ahead forecasts obtained in this manner for two dates, seven days apart, with the actual UK daily death numbers after the forecast origin (FO) shown as blue dots. These adaptive forecasts exploit an identified 15 day pure delay in the TF model, with the additional days forecast by the associated DHR model of the weekly cycle. As in the case of the Italy-UK analysis, there is clear evidence of parametric change in the model, so that adaptive, rolling forecasting of this kind is necessary.

5. Conclusions

The main objective of this paper has been to argue that continuous-time models describing the *input-output behaviour* of a stochastic, dynamic system have definite advantages when the physical nature of the system is as important as its forecasting behavior. Over many years, I have found it very strange that this model type is almost absent from the forecasting and time series analysis literature, particularly since such models are so important in science and engineering. Moreover, continuous-time modeling can be superior to discrete-time modeling, as shown in the case of climate model where the latter is unable to identify a model that can compete with the continuous-time model in either descriptive or statistical terms.

If continuous-time models are considered in the statistical literature they tend to be formulated in either the more complex and difficult stochastic differential

¹⁴Data obtained from <https://www.ecdc.europa.eu/en/publications-data?s=hospital+admissions>

equation form based on Itô calculus (see e.g. [21]); or a simpler but more limited nonlinear regression form, based on the *solution* of the differential equation (e.g. [20]), rather than on the identification of the differential equation itself, which is obviously more useful. I hope, therefore, that the examples discussed in this paper, together with the background material in Appendix A, may help to stimulate more interest in continuous-time model identification, estimation and practical application. I feel that such models are not only much easier to interpret in dynamic terms, they are also quite straightforward to estimate and use in forecasting applications, particularly when linked with other modeling tools of the unobserved component type, such as:

Dynamic Harmonic Regression.

This exploitation of Dynamic Harmonic Regression is very appropriate in this paper because it is dedicated to Antonio Garcia-Ferrer on his 70th birthday. Antonio, who is a much valued friend of many years, is a co-developer, with Marcos Bujosa, of the Linear Dynamic Harmonic Regression algorithm and they have exploited it in numerous successful applications.

Happy Birthday Antonio

Wendy and I hope you have many more of them and we are sorry we cannot be in Madrid with you and Pilar at this happy time.

Appendix A. Continuous Time Models & Methods

This appendix provides a brief outline of the continuous-time models used for the examples described in sections 3 and 4, as well as the statistical estimation tools used for their identification and estimation.

Appendix A.1. Hybrid Continuous-Time Transfer Function Models for Linear Systems

I was introduced to *Continuous-time Transfer Function* (CTF) models as a means to solving differential equations by my brother¹⁵, who suggested I read about them in the excellent book by Gardner and Barnes [8]. He suggested that this was much easier than the ‘complementary function - particular integral’ method I was struggling with at school. After a little tutoring from him, I found that he was entirely correct: the conversion of the problem into an entirely algebraic form, coupled and the many advantages of the CTF that resulted, convinced me that this was indeed the best approach and I have used it ever since.

For the present purposes, rather than provide a general introduction to CTF models, or more specifically to ‘hybrid CTF’ models (see later), it makes sense to consider an example that is identified from globally averaged climate data and is the subject of section 3 in the main part of the paper. Here, the CTF model takes the following hybrid form, where the main descriptive equation is in continuous-time form, while the additive noise is the well known, discrete time *AutoRegressive* (AR) model:

$$\begin{aligned} x_1(t) &= \frac{b_{10}}{s + a_{11}} u(t) && (i) \\ \text{Main CTF: } x_2(t) &= \frac{b_{20}s}{s^2 + a_{21}s + a_{22}} u(t - \tau) && (ii) \\ x(t) &= x_1(t) + x_2(t) && (iii) \quad (\text{A.1}) \\ \text{Noise: } \xi(k) &= \frac{1}{1 + c_1 z^{-1}} e(k) && (iv) \\ e(k) &= \mathcal{N}(0, \sigma^2) \\ \text{Output: } y(k) &= x(k) + \xi(k) && (v) \end{aligned}$$

In these equations, the ‘differential operator’ is $s^n = \frac{d^n}{dt^n}$, where n is the order of differentiation, e.g. $s^2 x(t) = \frac{d^2 x(t)}{dt^2}$ and $x(t)$ is the instantaneous value of the unobserved deterministic output at time t ; while the discrete-time

¹⁵11 years my senior and a notable electrical engineer (see [32, 33, 34, 35, 36]); to whom I am eternally grateful for his good advice and encouragement in my formative years and then throughout my life, until his untimely death in 1993.

'backward shift' operator is z^{-m} , where m is the number of shifts in sampling intervals, e.g. $z^{-1}\xi(k) = \xi(k-1)$ and $\xi(k)$ is the sampled value of the additive noise.

Note that I describe s^n as simply an operator and not as the 'Laplace transform' operator, to which it is intimately related. This because, although Laplace transform theory underlies all CTF models and, as outlined in Appendix B, it can be used to derive CTF models *that include the effects of initial conditions*, this is not essential to understanding the nature of the CTF model, nor in using the parameters in the model to expose the dynamic characteristics of the model *without solving the model equations*. Nor is it required in order to decompose the model into serial, parallel or feedback connections that often have physically meaningful interpretations. It is only if we wish to *manually* solve the equations that we have to know and understand this theory and, in particular, its 'inverse'. But this is hardly necessary these days because there are digital computer routines that can solve the equations for us: for example, given the CTF, the lsim routine in Matlab will solve the model equations for any specified inputs and initial conditions.

The main system model response $x(t)$ in (A.1)(iii) is a little unusual because the single input $u(t)$, representing the *Total Radiative Forcing* (TRF) in Wm^{-2} , affects the deterministic output $x(t)$, representing the *Global Temperature Anomaly* (GTA) in $^{\circ}C$, via two pathways: one, with response $x_1(t)$, has zero transportation delay; and the other, with response $x_2(t)$, has a delay of τ years. The sampled measurement $x(k)$ of $x(t)$ at the k th sampling instant is contaminated by 'noise' $\xi(k)$ to produce the observation $y(k)$ in (A.1)(v). $\xi(k)$ is identified as a discrete-time AR(1) model, which represents uncertainty of all forms in the measurements, ranging from random measurement noise to other, unexplained, perturbations in the measured response that are not being explained by the deterministic model output $x(t)$. As usual, the input $e(k)$ to this AR(1) model is assumed to be a zero mean, serially uncorrelated series of normally distributed random variables; and this assumption has to be checked following model parameter estimation.

The operational CTF form of the equations (A.1) can be converted easily into the hybrid differential equation form by cross multiplying the equations by the CTF denominator polynomials and allowing the operators in the polynomials to perform their appropriate function on the associated variable: e.g., separating out the first CTF in (A.1)(i), after simple cross-multiplication we obtain:

$$(s + a_{11})x_1(t) = b_{10}u(t) \quad (\text{A.2})$$

so that,

$$\frac{dx_1(t)}{dt} + a_{11}x_1(t) = b_{10}u(t) \quad (\text{A.3})$$

and, performing similar operations of the whole CTF model, yields the following three differential equations for the continuous-time components:

$$\frac{dx_1(t)}{dt} = -a_{11}x_1(t) + b_{10}u(t) \quad (\text{i})$$

$$\frac{d^2x_2(t)}{dt^2} = -a_{21}\frac{dx_2(t)}{dt} - a_{22}x_2(t) + b_{20}\frac{du(t-\tau)}{dt} \quad (\text{ii})$$

$$x(t) = x_1(t) + x_2(t) \quad (\text{iii})$$

The model is completed the following two equations for the discrete-time components at the k th sampling instant,

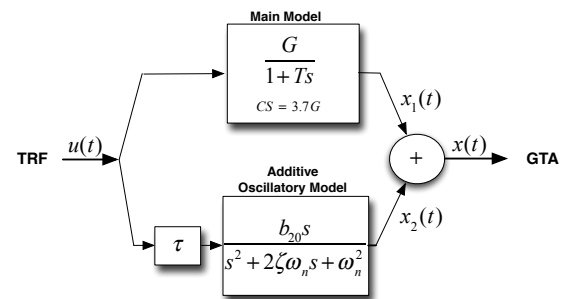
$$y(k) = x(k) + \xi(k) \quad (\text{i})$$

$$\xi(k) = -c_1\xi(k-1) + e(k) \quad (\text{ii})$$

$$e(k) = \mathcal{N}(0, \sigma^2) \quad (\text{A.5})$$

in which the argument k denotes that data are all sampled at a regular sampling interval Δt which, in the climate example, is one year.

In equations (A.1) and (A.4), $x_1(t)$ and $x_2(t)$ represent the outputs of the two pathways, shown in the 'block diagram' form of figure A.17, where the CTFs in the



$$G = 0.618; T = 19.3 \text{ y}; CS = 2.29; b_{20} = 0.0067; \tau = 17.5 \text{ y}$$

$$\omega_n = 0.0181 \text{ c/y; (period } 55.3 \text{ y); } \zeta = 0.036$$

Figure A.17: Block diagram of the final DBM model.

blocks are presented in a different way to those in equation (A.1) in order to explain the dynamic behavior of the CTF. This is a considerable advantage because the dynamic nature of the system can be inferred immediately from the parameters in this version of the model, *without having to resort to the solution of the underlying differential equation*.

Let us consider the 'derived' parameters in figure A.17 and how they are obtained from the estimated parameters in the model (A.1). In the case of the first CTF

in equation (A.1)(i), this first order model is defined completely by the following two ‘derived’ parameters shown in the upper pathway of figure A.17¹⁶:

$$\begin{aligned} \text{Steady State Gain: } G &= \frac{b_{11}}{a_{11}} \\ \text{Time Constant: } T &= \frac{1}{a_{11}} \end{aligned} \quad (\text{A.6})$$

As we shall see, both of these parameters have important implications in the present climate context, where G , is directly proportional to the *equilibrium Climate Sensitivity* (CS) that defines the equilibrium level of the globally averaged temperature (see main text); and T defines the time taken for the system to reach $1 - e^{-1} = 0.632$ of the final equilibrium level¹⁷.

The derived parameters shown in the second pathway of figure 4 are as follows:

$$\begin{aligned} \text{Steady State Gain: } G &= \frac{0}{a_{12}} = 0, \text{ in this case.} \\ \text{Natural Frequency: } \omega_n &= \sqrt{a_{22}} \text{ rad/time unit} \\ \text{Natural Period: } P_n &= \frac{2\pi}{\omega_n} \text{ time units} \\ \text{Damping Ratio: } \zeta &= \frac{a_{21}}{2\omega_n} = \frac{a_{21}}{2\sqrt{a_{22}}} \end{aligned} \quad (\text{A.7})$$

Once again, these parameters provide information on the system’s transient response characteristics. In this case, $G = 0$ because b_{21} is absent from the numerator and b_{20} is multiplying $s = \frac{d}{dt} = 0$ in the steady state (nothing is changing in the steady state) and so the steady state level of $x_2(t)$ is also zero. As regards any oscillatory response preceding the steady state, this occurs only¹⁸ if $\zeta < 1.0$. In this situation, oscillations occur at a frequency defined by the natural frequency ω_n radians/year, with an associated natural period $P_n = \frac{2\pi}{\omega_n}$ years; while if $\zeta = 0$, then the oscillations are undamped and the oscillatory response is sustained; and finally, for $0 < \zeta < 1.0$ (as in this climate model, where $\zeta = 0.036$), they are damped in time and die out unless the system is perturbed by a change in the input $u(t - \tau)$.

In this climate model case (see figure 4 and section 3, stage 4, of the main text), where $\omega_n = \sqrt{0.0129}$ radians/year or 0.0181 cycles/year; and $\zeta = 0.036$, the oscillations have a period of $P_n = 1/0.0181 = 55.3$ years

¹⁶In steady state equilibrium there is no change in the output, so $s = d/dt = 0$ and so, from (A.1)(i), $x_1(\infty) = \frac{b_{10}}{a_{11}} u(\infty)$.

¹⁷This has been termed ‘Feedback Response Time’ in climate publications: see section 3

¹⁸If $\zeta \geq 1.0$, the model has two real modes and so can be reduced to two first order, non-oscillatory CTFs, each defined as in (A.6).

and they die out very slowly because ζ , although positive, is very close to zero. Consequently, this second order model accounts for the behaviour of the important oscillatory component of the GTA discussed in the main text. Another model of this second order form, but with b_{21} present, is mentioned briefly in section 3 of the main text. This characterizes the relationship between $x_2(t)$ and the well known *Atlantic Multidecadal Oscillation*. However, the full details of this model and its estimation are given in [50].

Finally, it should be noted that it sometimes assists in the physical interpretation of the model to decompose a second order equation such as that in (A.1)(ii) into a *feedback* connection of two first order CTFs. This is possible if the TFdecomp routine in CAPTAIN computes a physically meaningful decomposition into the two first order systems, each defined as in (A.6). The climate example of such a feedback decomposition relates to the feedback decomposition of equation (A.1)(ii) and this is discussed in section 3, stage 4, of the main text.

Appendix A.2. Hybrid Continuous-Time Model Identification and Estimation

The statistical identification and estimation of the continuous-time models outlined in the previous section is too large a topic to be discussed in detail within the present paper. Suffice it to say the methodology has been developed over many years, starting with the estimation of such models on analog and hybrid (combined analog-digital) computers in the 1960s (see e.g. [37, 38]) and figure A.18, below. However, their optimal

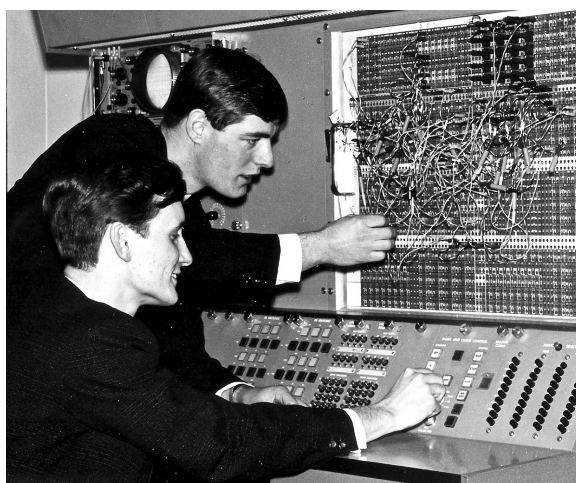


Figure A.18: The author (seated) and Colin Dwyer using a hybrid computer for continuous-time model estimation: Loughborough University, UK, 1965.

estimation on a digital computer was first considered sometime later with the development of the *Refined Instrumental Variable* (RIV) method of estimating parameters in transfer function models [39] and its application to continuous-time models (RIVC) shortly afterwards [46]. The latest, definitive description of RIV/RIVC estimation [42] has shown how this approach can be considered as the maximum likelihood estimation of a unified Box-Jenkins model¹⁹ that accommodates both continuous and discrete-time models. The RIV/RIVC optimization is carried out using a rapidly convergent iterative method that Vic Solo²⁰ has entitled *Pseudo-Linear Regression* (PLR) and which has been shown [42, 30] to be a special ‘damped’ example of a Gauss-Newton optimization algorithm [16]. Other related research and development, including the estimation of such models in a closed loop system [9] and the extension to partial differential equation models [27], has been considered over the last 20 years (see also [31, 10] and the prior references therein).

In simple terms, RIV/RIVC estimation provides a robust approach to optimal estimation of parameters in both continuous-time and discrete-time transfer function models (and thus the same parameters in the associated differential and difference equations). It is robust because it employs an optimal method of instrumental variable estimation that ensures consistent (asymptotically unbiased) estimation of the parameters *even if the assumptions about the additive noise are not satisfied*.

Indeed, RIV/RIVC estimation can always be used without the inclusion of a noise model, so that the objective is simply the minimization of the output error $y(k) - \hat{x}(k)$: it is then referred to as the *Simplified Refined IV* (SRIVC or SRIV) algorithm. These simplified algorithms are useful at the model structure identification stage of the modeling process. This naturally precedes rivcbj and rivbj estimation and is facilitated by the rivcbjid and rivbjid routines in CAPTAIN. These identify the best structure and are based on a user-specified range of model orders and order identification criteria, such as the AIC, BIC [2, 28] and YIC [40].

When the statistical assumptions are justified, however, the noise can be modeled as an *AutoRegressive Moving Average* (ARMA) process, and then the estimation is also optimal in a maximum likelihood sense and the parameter estimates are asymptotically efficient

(minimum variance). It is interesting to note that, although most of this research and development has been carried out within a dynamic systems and control context, the RIV/RIVC method depends for its success on the theorem of Pierce [23], which shows that the estimation of the system and noise models are asymptotically independent, thus simplifying the model structure identification and parameter estimation procedures. In CAPTAIN, there are routines available for both continuous (rivcbj) and discrete-time (rivbj) TF models, so covering all the major models in the hybrid Box-Jenkins family²¹.

Finally, it is worth noting that the identification of a complete discrete-time model, of the kind used currently in most forecasting applications, is problematical if the sampling rate is too fast. This is because the model does not ‘see’ longer period behaviour well and so this is poorly identified. One solution is to sample the data more coarsely and this is discussed briefly in section 3.2 of the main text. This shows that the higher parametric uncertainty caused by the reduced sample size, as well as limitations in the nature of the higher order identified model, mean that the resulting climate model has to be rejected as unsatisfactory when compared with the differential equation model, which is very much better defined in statistical terms.

Appendix A.3. Unobserved Component models and Dynamic Harmonic Regression

The *Dynamic Harmonic Regression* (DHR) algorithm [49] has become the most popular algorithm in the CAPTAIN Toolbox and, together with the closely related Linear DHR algorithm, developed by Professor Antonio Garcia Ferrer and Dr. Marcos Bujosa [6], it has very wide application potential. It is now used by many people around the World for analyzing and forecasting time series, particularly those exhibiting periodic behaviour. For example, it is very popular within the environmental science community; while Antonio and Marcos have made continuing and very successful use of this flexible algorithm in an economic context (see e.g. [5]) to predict recessions using the factor linear DHR algorithm.

The DHR model is best considered as an implementation of the *Unobserved Component* (UC) model, where the sampled observed series $y(k)$, at sampling instant k ,

¹⁹The discrete-time model suggested by Box and Jenkins and first described in their 1970 book [4].

²⁰Professor Solo is a long-time friend and former research student, who worked on recursive estimation with Professor Ted Hannan and myself, at the Australian National University in the 1970s

²¹Note that it is possible to implement a related algorithm for the δ -operator TF model where δ , defined as $\delta = \frac{s-1}{\Delta t}$, is the discrete-time equivalent of the continuous-time s operator. However, this is normally used in an automatic control context.

is considered as the sum of unobserved components, i.e,

$$\begin{aligned} y(k) &= T(k) + f\{\mathbf{u}(k)\} + W(k) + e(k) \\ e(k) &= \mathcal{N}(0, \sigma^2) \end{aligned} \quad (\text{A.8})$$

Here, $T(k)$ is a normally a smooth, low frequency ‘trend’ component; $f\{\mathbf{u}(k)\}$ is a function of any input variables $\mathbf{u}(k) = [u_1(k) \ u_2(k) \ \dots \ u_n(k)]$ that affect the system, normally via hybrid continuous-time TF models of the kind discussed in Appendix A.1 above; while $W(k)$ is an underlying continuous-time cyclical component composed of sine and cosine functions modulated by *time variable* parameters, i.e. the underlying continuous-time model is as follows:

$$W(t) = \sum_{i=1}^{R_c} \{\alpha(i, t) \cos(\omega_i t) + \beta(i, t) \sin(\omega_i t)\} \quad (\text{A.9})$$

where ω_i , $i = 1, 2, \dots, R_s$, are the fundamental and harmonic frequencies associated with the cyclicity in the series. The irregular component $e(k)$ in (A.8) represents the stochastic variations in $y(k)$ that have not been explained by all the other components: normally, if the spectral peaks have been identified well, then it will be a zero mean, normally distributed and serially uncorrelated, white noise process.

Each *Time Variable Parameter* (TVP), $\alpha(i, t)$ and $\beta(i, t)$ in (A.9) is programmed to be one member of the *Generalized Random Walk* (GRW) family. This GRW family includes a number of special cases (see [40]) but the most important of these are the vector *Integrated Random Walk* (IRW); the scalar *Random Walk*; and the intermediate case of the vector *Smoothed Random Walk* (SRW). The estimated frequency values are chosen by reference to the spectral properties of the time series, as quantified by the AR(n) spectrum, with the order n identified by reference to the *Akaike Information Criterion* (AIC: see [1]).

This DHR model can be considered as a straightforward extension of the classical, constant parameter, harmonic regression (Fourier series) model, in which the gain and phase of the harmonic components are allowed to vary over time if this is identified from the time series data in the form of temporal changes in the estimated parameters $\alpha(i, t)$ and $\beta(i, t)$. These are normally estimated at the regular sampling instants $k = 1, 2, \dots, N$, where N is the total number of samples in the time series. However, because the sines and cosines are defined continuous-time variables, the DHR algorithm can be applied to an irregularly sampled series [19] and the `as-dhr` routine for doing this will be available shortly in CAPTAIN.

There are hyper-parameters associated with the GRW models and these are optimized, normally using the `dhrpt` routine in CAPTAIN, so that model spectrum matches the AIC optimized AR(n) spectrum: in effect, the optimized TVPs allow the spectral peaks to be shaped to match the empirical AR spectrum. The DHR algorithm is formulated in fully recursive terms based on the *Kalman Filter* (KF) and *Fixed Interval Smoothing* (FIS) algorithms. Here, the KF implements standard TVP filtering, so that it can provide forecasts by simply specifying missing data from the end of the time series for the length of the required forecast; while the FIS algorithm allows for optimally smoothed estimation, where the estimate at each sampling instant is based on all the available data, so providing the ability to *interpolate* over missing samples in the time series. This DHR algorithm is implemented in CAPTAIN²² as the `dhr` routine and the missing data required for interpolation and forecasting are specified in the series by the Matlab ‘not-a-number’ NaN. Other routines required in the DHR analysis are the `aic`, for identifying the optimal AR model order; and `arspec` to define the position of the peaks in this AR spectrum.

Appendix B. Estimating Initial Condition Effects in RIVC Estimation

The best way to illustrate how initial conditions can be accounted for in RIVC estimation is to consider the following first order differential equation model:

$$\frac{dx(t)}{dt} + a_1 x(t) = b_0 \frac{du(t)}{dt} + b_1 u(t) \quad (\text{B.1})$$

The Laplace transform of this model (see e.g. [14]) yields:

$$sx(s) + x(0) + a_1 x(s) = b_0 su(s) + u(0) + b_1 u(s) \quad (\text{B.2})$$

where $x(0)$ and $u(0)$ are the initial conditions on $x(t)$ and $u(t)$, respectively. Consequently the associated CTF model is as follows:

$$x(s) = \frac{b_0 s + b_1}{s + a_1} u(s) + \frac{u(0) - x(0)}{s + a_1} 1.0 \quad (\text{B.3})$$

As a result, it is straightforward to incorporate an allowance for initial condition effects into the RIVC algorithm by adding an additional constant input set to unity over the whole observational interval. The initial

²²without the $f\{\mathbf{u}(k)\}$ component which needs to be added using customized coding because it is difficult to generalize.

conditions are then estimated as the parameter(s) of the second TF in (B.3) that is associated with this additional input (here, a single parameter defined by $u(0) - x(0)$); and the output of this TF adds a response to the output that accounts for the effects of the initial conditions. This ensures a better explanation of the data over the time it takes for the effects of the initial conditions to decay. This time can be considerable in some cases, so accounting for the initial condition effects can be very important, as shown in section 3 of the main text. Finally, note that it may be necessary in practice to increase the order of the numerator in the second TF to fully account for the initial condition effects.

Bibliography

- [1] H. Akaike. A new look at statistical model identification. *IEEE Transactions on Automatic Control*, 19:716–723, 1974.
- [2] H. Akaike. A Bayesian extension of the minimum AIC procedure of autoregressive model fitting. *Biometrika*, 66:237–242, 1979.
- [3] D. G. Andrews and M. R. Allen. Diagnosis of climate models in terms of transient climate response and feedback response time. *Atmospheric Science Letters*, 9:7–12, 2007.
- [4] G. E. P. Box and G. M. Jenkins. *Time Series Analysis Forecasting and Control*. Holden-Day: San Francisco, 1970.
- [5] M. Bujosa, A. García-Ferrer, and A. De-Juan. Predicting recessions with factor linear dynamic harmonic regressions. *Journal of Forecasting*, 32:481–499, 2013.
- [6] M. Bujosa, A. García-Ferrer, and Peter C. Young. Linear dynamic harmonic regression. *Computational Statistics & Data Analysis*, 52:999–1024, 2007.
- [7] F. Chen and P. C. Young. A simple robust method of fractional time delay estimation for linear dynamic systems. *submitted for publication*, 2019.
- [8] M. F. Gardner and J. L. Barnes. *Transients in linear systems studied by the Laplace transformation*. J. Wiley and Sons, New York, 1942.
- [9] H. Garnier, L. Wang, and P. C. Young. Direct identification of continuous-time models from sampled data: issues, basic solutions and relevance. In H. Garnier and L. Wang, editors, *Identification of Continuous-Time Models from Sampled Data*, pages 1–29. Springer-Verlag: London, 2008.
- [10] M. Gilson, H. Garnier, P.C. Young, and P. Van den Hof. Optimal instrumental variable methods for closed-loop identification. *IET Control Theory & Applications*, 5(10):1147–1154, July 2011.
- [11] A. J. Jarvis, P. C. Young, D. T. Leedal, and A. Chotai. A robust sequential CO_2 emissions strategy based on optimal control of atmospheric CO_2 concentrations. *Climate Change*, 86:357–373, 2008.
- [12] R. Knutti et al. Comment on “heat capacity, time constant, and sensitivity of earth’s climate system” by S. E. Schwartz. *Journal of Geophysical Research*, 113:D15103, 2008.
- [13] T. Kuhn. *The Structure of Scientific Revolutions*. University of Chicago, Chicago, 1962.
- [14] Benjamin C. Kuo and Farid Golnaraghi. *Automatic Control Systems*. John Wiley & Sons, Inc., New York, NY, USA, 2002.
- [15] C. M. Liaw. Model reduction of discrete systems using the power decomposition method. *Proc. Inst. of Electrical Engineers*, 133, Pt.D:30–34, 1986.
- [16] L. Ljung. *System identification. Theory for the user*. Prentice Hall, Upper Saddle River, N.J., 2nd edition, 1999.
- [17] M. Meinshausen, S. C. B. Raper, and T. M. L. Wigley. Emulating coupled atmosphere-ocean and carbon cycle models with a simpler model, MAGICC6 – Part 1: Model description and calibration. *Atmos. Chem. Phys.*, 11:417–1456, 2011.
- [18] Malte Meinshausen, S. J. Smith, K. Calvin, J. S. Daniel, M. L. T. Kainuma, J-F. Lamarque, K. Matsumoto, S. A. Montzka, S. C. B. Raper, K. Riahi, A. Thomson, G. J. M. Velders, and D.P. P. van Vuuren. The rcp greenhouse gas concentrations and their extensions from 1765 to 2300. *Climatic Change*, 109(1):213, Aug 2011.
- [19] D. A. Mindham and W. Tych. Dynamic harmonic regression and irregular sampling: avoiding pre-processing and minimising modelling assumptions. *Environmental Modelling and Software*, page 121, 2019.
- [20] E. Myrvoll-Nilsen, S. H. Sørbye, H. Fredriksen, H. Rue, and M. Rydpdal. Statistical estimation of global surface temperature response to forcing under the assumption of temporal scaling. *Earth System Dynamics*, 11:329–345, 2019.
- [21] J.N. Nielsen, H. Madsen, and P.C. Young. Parameter estimation in stochastic differential equations: an overview. *Annual Reviews in Control*, 24:83–94, 2000.
- [22] S. Parkinson and P. C. Young. Uncertainty and sensitivity in global carbon cycle modelling. *Climate Research*, 9:157–174, 1998.
- [23] D. A. Pierce. Least squares estimation in dynamic disturbance time-series models. *Biometrika*, 5:73–78, 1972.
- [24] Karl Popper. *The Logic of Scientific Discovery*. Hutchinson, London, 1959.
- [25] D. A. Randall et al. Climate models and their evaluation. In S. Solomon, D. Qin et al, editor, *Climate Change 2007: The Physical Science Basis. Contribution of Working Group I to the Fourth Assessment Report of the Intergovernmental Panel on Climate Change*, pages 589–662, Cambridge, United Kingdom and New York, NY, USA, 2007. Cambridge University Press.
- [26] M. Schlesinger and N. Ramankutty. An oscillation in the global climate system of period 65–70 years. *Nature*, 367:723–726, 1994.
- [27] J. Schorsch, H. Garnier, M. Gilson, and P. C. Young. Instrumental variable methods for identifying partial differential equation models. *International Journal of Control*, 86:2325–2335, 2013.
- [28] G. Schwarz. Estimating the dimension of a model. *Annal. Statist.*, 6:461–464, 1978.
- [29] S. Shackley, P. C. Young, S. Parkinson, and B. Wynne. Uncertainty, complexity and concepts of good science in climate change modelling: are GCMs the best tools? *Climatic Change*, 38:159–205, 1998.
- [30] P. Van den Hof and S.G. Douma. An IV-based iterative linear regression algorithm with optimal output error properties. Technical Report 09-018, Delft Center for Systems and Control, Delft University of Technology, 2008.
- [31] L. Wang and H. Garnier, editors. *System Identification, Environmetric Modelling and Control System Design*. Springer, U.K., 2011.
- [32] J. F. Young. *Applied Electronics*. Iliffe, London, 1968.
- [33] J. F. Young. *Cybernetics*. Iliffe Books Ltd., London, 1969.
- [34] J. F. Young. *Information Theory*. Butterworth, London, 1971.
- [35] J. F. Young. *Cybernetic Engineering*. John Wiley and Sons, 1973.
- [36] J. F. Young. *Robotics*. Butterworths, London, 1973.
- [37] P. C. Young. The determination of the parameters of a dynamic process. *Radio and Electronic Eng. (Jnl. of IERE)*, 29:345–361, 1965.
- [38] P. C. Young. Process parameter estimation and self adaptive con-

- trol. In P. H. Hammond, editor, *Theory of Self Adaptive Control Systems*, pages 118–140. Plenum Press: New York, 1966.
- [39] P. C. Young. Some observations on instrumental variable methods of time-series analysis. *International Journal of Control*, 23:593–612, 1976.
- [40] P. C. Young. *Recursive Estimation and Time-Series Analysis: An Introduction for the Student and Practitioner*. Springer-Verlag, Berlin., 2011.
- [41] P. C. Young. Hypothetico-inductive data-based mechanistic modeling of hydrological systems. *Water Resources Research*, 49(2):915–935, 2013.
- [42] P. C. Young. Refined instrumental variable estimation: Maximum likelihood optimization of a unified Box-Jenkins model. *Automatica*, 52:35–46, 2015.
- [43] P. C. Young. Data-based mechanistic modelling and forecasting globally averaged surface temperature. *International Journal of Forecasting*, 34:315–334, 2018.
- [44] P. C. Young. Additional material for the paper monitoring and forecasting the covid-19 epidemic in the UK. Technical report, Lancaster University Environment Centre and the Data Science Institute (available from author: email p.young@lancaster.ac.uk), 2020.
- [45] P. C. Young, P. G. Allen, and J. T. Bruun. A re-evaluation of the Earth’s surface temperature response to radiative forcing. *Environmental Research Letters*, 16(5):054068, 2021.
- [46] P. C. Young and A. J. Jakeman. Refined instrumental variable methods of time-series analysis: Part III, extensions. *International Journal of Control*, 31:741–764, 1980.
- [47] P. C. Young, A. J. Jakeman, and R. McMurtrie. An instrumental variable method for model order identification. *Automatica*, 16:281–296, 1980.
- [48] P. C. Young and A. J. Jarvis. Data-based mechanistic modelling, the global carbon cycle and global warming. Technical Report TR 177, Centre for Research in Environmental Systems and Statistics (CRES), Lancaster University, 2002.
- [49] P. C. Young, D. J. Pedregal, and W. Tych. Dynamic harmonic regression. *Journal of Forecasting*, 18:369–394, 1999.
- [50] Peter C. Young. Hypothetico-inductive DBM modelling of globally averaged surface temperature and the estimation related climate parameters. LEC technical report 2019 (available from author p.young@lancaster.ac.uk), Lancaster Environment Centre: Lancaster University, UK, 2019.
- [51] Peter C. Young and Fengwei Chen. Monitoring and forecasting the covid-19 epidemic in the uk. *Annual Reviews in Control*, 51:488–499, 2021.